Lewellyn et al., http://www.jcb.org/cgi/content/full/jcb.201008138/DC1

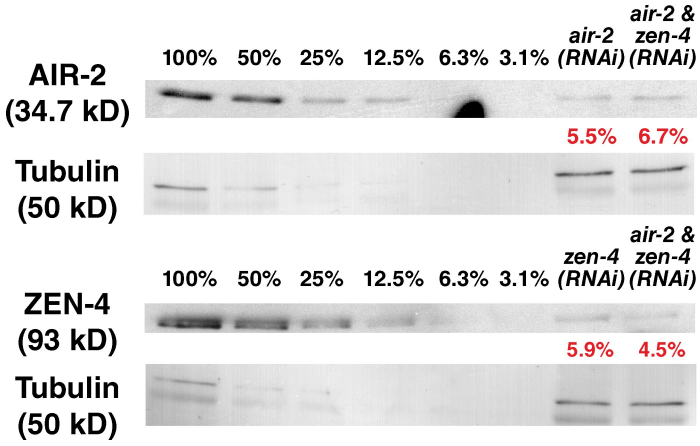

Figure S1. **Western blot of control, *air-2(RNAi)*, *zen-4(RNAi)*, and *air-2 & zen-4(RNAi)* worms.** Serial dilutions of a control lysate made from uninjected N2 worms (percentage of amount in 100% control indicated above each lane) were used to quantify the amount of Aurora B^{AIR-2} or MKLP1^{ZEN-4} in the RNAi samples (two right lanes). The Western blot was analyzed by drawing a box around each band and measuring the signal above background. The signals from the serial dilution of the control lysate were used to generate a standard curve that was used to calculate the amount in the RNAi lanes (red; expressed as a percentage of the amount in the 100% control lane).

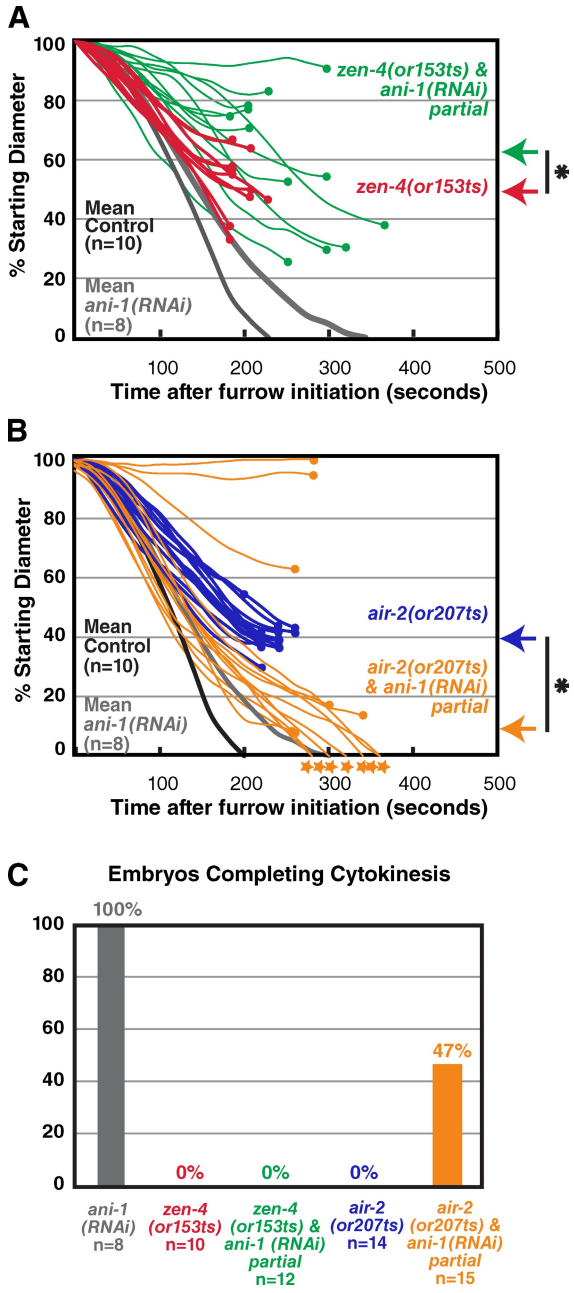

Figure S2. **The contractile ring constriction defect in Aurora B^{AIR-2}–inhibited embryos is alleviated by partial depletion of anillin^{ANI-1}.** Because anillin^{ANI-1} is required to target the septins to the ring, we tested whether anillin^{ANI-1} depletion could alleviate the constriction defect resulting from postmeiotic upshift of *air-2(or207ts)* mutant embryos. Anillin is upstream of the septins in the contractile ring assembly pathway, and its depletion has a more deleterious effect on other cortical events, including polar body extrusion, cortical ruffling, and pseudocleavage, than the septins (Maddox et al., 2005). We therefore tested the effect of partial anillin^{ANI-1} depletion (dsRNA injected ~24 h before imaging) on constriction. As for septin^{UNC-59} depletion, partial anillin depletion enhanced the constriction defect in the upshifted *zen-4(or153ts)* mutant embryos and significantly suppressed the constriction defect in upshifted *air-2(or207ts)* mutant embryos. (A and B) Traces of furrow diameter versus time for individual *zen-4(or153ts)* and *zen-4(or153ts) & ani-1(RNAi) partial* embryos (A) or *air-2(207ts)* and *air-2(207ts) & ani-1(RNAi) partial* embryos. Furrow diameters in A and B were measured in end-on projections of 11-plane z series collected every 20 s. Traces were smoothed by applying a three-point rolling mean. The circles mark the final diameter before regression. The stars at the end of the trace indicate successful completion of cytokinesis. The arrows to the right of the graphs mark the mean maximum ingression for the indicated conditions. For comparison, mean contractile ring diameter is plotted versus time for control and *ani-1(RNAi)* embryos. The control, *zen-4(or153ts)*, and *air-2(or207ts)* traces are the same as those shown in Fig. 5. The asterisks indicate significant differences (two-tailed *t* test, $P < 0.05$). (C) For embryos analyzed in the single experiment in A and B (n = 8–15 embryos per condition), the percentages of embryos that completed cytokinesis are shown. All imaging was performed using the postmeiotic upshift conditions outlined in Fig. 2 A.

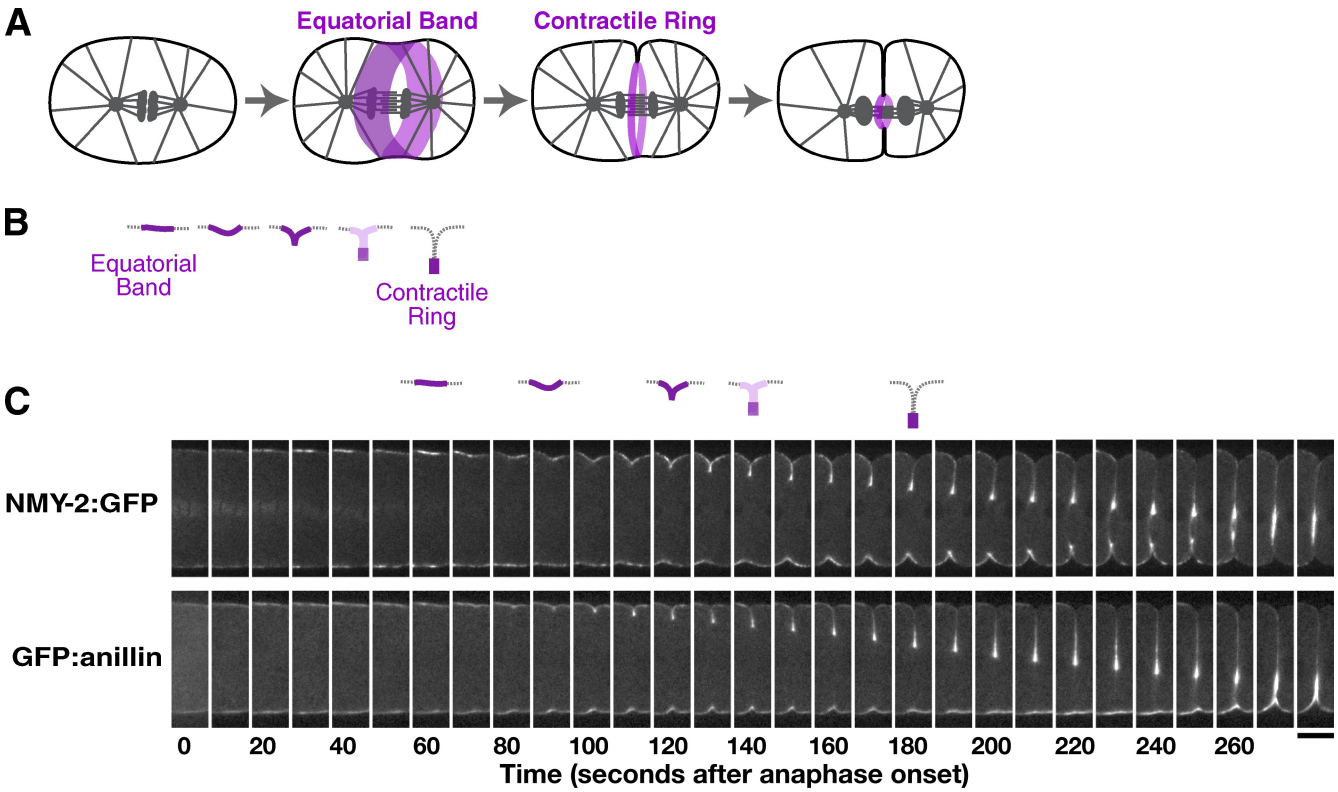

Figure S3. **Contractile ring assembly occurs in two steps.** (A and B) The schematics (reproduced from Fig. 7, A and B) illustrate the steps in cytokinesis. In an initial step, contractile ring proteins accumulate in a broad equatorial band that encircles the cell equator. In a second step, the cortex folds in, and contractile ring proteins become concentrated in a compact ring that sits at the furrow tip and are cleared from the remainder of the equatorial cortex (illustrated in B). (C) Montages of the equatorial region in central plane confocal images of control embryos expressing NMY-2:GFP (top) and GFP:anillin (bottom) show a side view of the equatorial band and its conversion to the compact contractile ring. Bar, 10 µm.

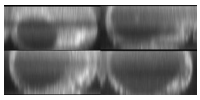

Video 1. **Simultaneous depletion of Aurora B^{AIR-2} and MKLP1^{ZEN-4} leads to an additive contractile ring constriction defect.** Examples of *C. elegans* control, *zen-4(RNAi)*, *air-2(RNAi)*, and *air-2 & zen-4(RNAi)* embryos expressing a GFP plasma membrane probe (white). End-on reconstructions of the division plane from 11 × 2.5–µm z series collected every 20 s starting at the time of the initial deformation of the cortex. Images were acquired using a spinning disk confocal system mounted on an inverted microscope. Playback rate is 120× real time.

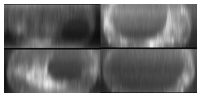

Video 2. **Codepletion of Aurora B^{AIR-2} and MKLP1^{ZEN-4} in the upshifted double mutant results in an additive contractile ring constriction defect versus depletion of Aurora B^{AIR-2} or MKLP1^{ZEN-4} alone in the corresponding upshifted single mutants.** Examples of *C. elegans* control, *zen-4(RNAi);zen-4(or153ts)*, *air-2(RNAi);air-2(or207ts)*, and *air-2 & zen-4(RNAi);air-2(or207ts)zen-4(or153ts)* embryos expressing a GFP plasma membrane probe (white). End-on reconstructions of the division plane from 11 × 2.5–µm z series collected every 20 s starting at the time of the initial deformation of the cortex. Images were acquired using a spinning disk confocal system mounted on an inverted microscope. Playback rate is 120× real time.

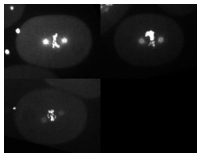

Video 3. **A temperature-sensitive Aurora B^{AIR-2} mutant can be used to bypass the meiotic defects resulting from CPC inhibition.** Control, *air-2(RNAi)*, and *air-2(or207ts)* embryos expressing GFP:tubulin and GFP:histone H2B (white) were imaged every 5 s starting at NEBD. Imaging was performed using the postmeiotic upshift conditions outlined in Fig. 2 A. Images are maximum intensity projections of 5 × 2–µm z series acquired using a spinning disk confocal system mounted on an inverted microscope. Playback rate is 50× real time.

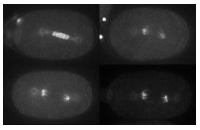

Video 4. **Aurora B^{AIR-2} localizes to microtubules emanating from the chromosomes into the region between the separating chromosomes in *C. elegans* embryos depleted of $PRC1^{SPD-1}$ or $MKLP1^{ZEN-4}$.** Single central confocal images of control, *spd-1(RNAi)*, *zen-4(RNAi)*, and *spd-1 & zen-4(RNAi)* embryos expressing GFP:Aurora B^{AIR-2} (white) were acquired at 10-s intervals. Videos begin at metaphase. Images were acquired using a spinning disk confocal system mounted on an inverted microscope. Playback rate is 60× real time.

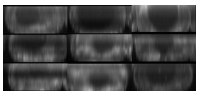

Video 5. **Cytokinesis completes successfully in *C. elegans* embryos depleted of $septin^{UNC-59}$ or $anillin^{ANI-1}$.** Three examples of control, *unc-59(RNAi)*, and *ani-1(RNAi)* embryos expressing the GFP plasma membrane probe (white) are shown. End-on reconstructions of the division plane from 11 × 2.5–μm z series collected every 20 s. Images were acquired using a spinning disk confocal system mounted on an inverted microscope. Playback rate is 120× real time. Imaging was performed using the postmeiotic upshift conditions outlined in Fig. 2 A.

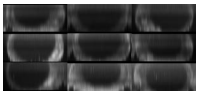

Video 6. **Depletion of $septin^{UNC-59}$ or partial depletion of $anillin^{ANI-1}$ alleviates the constriction defect in Aurora B^{AIR-2}–inhibited *C. elegans* embryos.** Three examples of *air-2(or207ts)*, *air-2(or207ts);unc-59(RNAi)*, and *air-2(or207ts);ani-1(RNAi) partial* embryos expressing the GFP plasma membrane probe (white) are shown. End-on reconstructions of the division plane from 11 × 2.5–μm z series collected every 20 s starting at the time of the initial deformation of the cortex. Images were acquired using a spinning disk confocal system mounted on an inverted microscope. Playback rate is 120× real time. Imaging was performed using the postmeiotic upshift conditions outlined in Fig. 2 A.

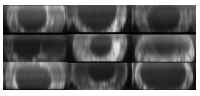

Video 7. **Depletion of $septin^{UNC-59}$ or partial depletion of $anillin^{ANI-1}$ does not alleviate the constriction defect in *C. elegans zen-4(or153ts)* embryos.** Three examples of *zen-4(or153ts)*, *zen-4(or153ts);unc-59(RNAi)*, and *zen-4(or153ts);ani-1(RNAi) partial* embryos expressing the GFP plasma membrane probe (white) are shown. End-on reconstructions of the division plane from 11 × 2.5–μm z series collected every 20 s starting at the time of the initial deformation of the cortex. Images were acquired using a spinning disk confocal system mounted on an inverted microscope. Playback rate is 120× real time. Imaging was performed using the postmeiotic upshift conditions outlined in Fig. 2 A.

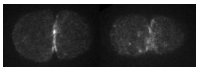

Video 8. **Codepletion of centralspindlin and the CPC does not affect recruitment of GFP:$anillin^{ANI-1}$ to the equatorial band.** Spinning disk confocal optics were used to collect images of the cortex in *C. elegans* control and *zen-4 & air-2(RNAi)* embryos expressing GFP:$anillin^{ANI-1}$ (white). A 4 × 1–μm z series containing the embryo cortex was collected every 20 s beginning 160 s after NEBD, and a maximum intensity projection was generated for each time point. Images were acquired using a spinning disk confocal system mounted on an inverted microscope. Playback rate is 120× real time.

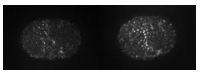

Video 9. **Codepletion of centralspindlin and the CPC does not affect recruitment of NMY-2:GFP to an equatorial band.** Spinning disk confocal optics were used to collect images of the cortex in *C. elegans* control and *zen-4 & air-2(RNAi)* embryos expressing NMY-2:GFP (white). A 4 × 1–μm z series containing the embryo cortex was collected every 20 s beginning 120 s after NEBD, and a maximum intensity projection was generated for each time point. Images were acquired using a spinning disk confocal system mounted on an inverted microscope. Playback rate is 120× real time.

Table S1. **Worm strains used in this study**

Strain no.	Genotype	Reference
N2 (ancestral)		
OD27	unc-119(ed3) III; ltIs14 [pASM05; pie-1/GFP-TEV-STag::AIR-2;unc-119 (+)]	Canman et al., 2008
OD38	unc-119(ed3) III; ltIs28 [pASM14; pie-1/GFP-TEV-STag::ANI-1; unc-119 (+)]	Maddox et al., 2007
JJ1473	unc-119(ed3) III; zuIs45[nmy-2::NMY-2::GFP + unc-119(+)] V	Nance et al., 2003
EU554	zen-4(or153ts) IV	Severson et al., 2000
EU630	air-2(or207ts) I	Severson et al., 2000
OD95	unc-119(ed3) III; ltIs37 [pAA64; pie-1/mCHERRY::his-58; unc-119 (+)] IV; ltIs38 [pAA1; pie-1/GFP::PH(PLC1delta1); unc-119 (+)]	Canman et al., 2008
OD106	unc-119(ed3)III; zen-4(or153ts) IV; ltIs38 [pAA1; pie-1/GFP::PH(PLC1delta1); unc-119 (+)]	This study
OD52	unc-119(ed3) ruIs32[pAZ132; pie-1/GFP::histone H2B] III; ltIs24 [pAZ132; pie-1/GFP::tba-2; unc-119 (+)]	This study
OD253	air-2(or207ts) I; unc-119(ed3) ruIs32[pAZ132; pie-1/GFP::histone H2B] III; ltIs24 [pAZ132; pie-1/GFP::tba-2; unc-119 (+)]	This study
OD105	air-2(or207ts) I; unc-119(ed3) III; ltIs38 [pAA1; pie-1/GFP::PH(PLC1delta1); unc-119 (+)]	Canman et al., 2008
OD488	air-2(or207ts) I; unc-119(ed3) III; zen-4(or153ts) IV; ltIs38 [pAA1; pie-1/GFP::PH(PLC1delta1); unc-119 (+)]	This study
OD236	zen-4(or153ts)IV; zuIs45[nmy-2::NMY-2::GFP + unc-119(+)]V	Canman et al., 2008
OD283	air2(or207ts)I; zuIs45[nmy-2::NMY-2::GFP + unc-119(+)]V	This study

Table S2. **dsRNAs used in this study**

Gene	Oligonucleotide 1	Oligonucleotide 2	Template	RNA concentration
				mg/ml
Y34D9A.4 (*spd-1*)	TAATACGACTCACTATAGGTCGTTGACG CGTACTCAACT	AATTAACCCTCACTAAAGGGAATTCG AAATCCGACTCCA	N2 genomic	3.11
B0207.4 (*air-2*)	AATTAACCCTCACTAAAGGTTTCGAGAT CGGAAGACCAC	TAATACGACTCACTATAGGCAACGAC AAGCAATCTTCCA	yk483g8	1.49
M03D4.1 (*zen-4*)	AATTAACCCTCACTAAAGGAATTGGTTA TGGCTCCGAGA	TAATACGACTCACTATAGGATTGGAG CTGTTGGATGAGC	yk35d10	1.28
W09C5.2 *(unc-59)*	TAATACGACTCACTATAGGCGTGAAAC TCGTGGAGAACA	AATTAACCCTCACTAAAGGTTGTGGT GGAGTTCAACGTG	yk465c12	1.95
T03F1.9 *(hcp-4)*	AATTAACCCTCACTAAAGGGGAAATGT ACGGAGCGAAAA	TAATACGACTCACTATAGGACATTGTT GGTGGGTCCAAT	N2 genomic	1.36
C10H11.9 *(let-502)*	TAATACGACTCACTATAGGCCAGGATC CTCGTCATTTGT	AATTAACCCTCACTAAAGGTCGGTTTT TCGAGTCCAACT	N2 genomic	1.65
C06C3.1 *(mel-11)*	AATTAACCCTCACTAAAGGAAAAGGA GCCGATGTGAATG	TAATACGACTCACTATAGGTCGTTTCC GTTCACTTGTCA	N2 genomic	2.7
Y48E1B.12 *(csc-1)*	AATTAACCCTCACTAAAGGACCACGC AAGATCAAGAAGG	TAATACGACTCACTATAGGTATACAGA CGTCCCGGCATT	N2 genomic	0.48
F11H8.4 *(cyk-1)*	TAATACGACTCACTATAGGGGGCATTCT TCAAGGATCAA	AATTAACCCTCACTAAAGGTGGTGAG ATTTGCGATGTTC	yk576g9	2.59
C09G12.8 *(ced-10)*	TAATACGACTCACTATAGGTCAAATGTG TCGTCGTTGGT	AATTAACCCTCACTAAAGGATCGCCT CATCGAAAACTTG	N2 cDNA	1.0
Y49E10.19 *(ani-1)*	TAATACGACTCACTATAGGTCAAACTCA ATGGAGAGGACAA	AATTAACCCTCACTAAAGGCATTGTG CTTCAAATTCCTCAC	yk488c11	2.18

References

Canman, J.C., L. Lewellyn, K. Laband, S.J. Smerdon, A. Desai, B. Bowerman, and K. Oegema. 2008. Inhibition of Rac by the GAP activity of centralspindlin is essential for cytokinesis. *Science*. 322:1543–1546. doi:10.1126/science.1163086

Maddox, A.S., B. Habermann, A. Desai, and K. Oegema. 2005. Distinct roles for two *C. elegans* anillins in the gonad and early embryo. *Development*. 132:2837–2848. doi:10.1242/dev.01828

Maddox, A.S., L. Lewellyn, A. Desai, and K. Oegema. 2007. Anillin and the septins promote asymmetric ingression of the cytokinetic furrow. *Dev. Cell*. 12:827–835. doi:10.1016/j.devcel.2007.02.018

Nance, J., E.M. Munro, and J.R. Priess. 2003. *C. elegans* PAR-3 and PAR-6 are required for apicobasal asymmetries associated with cell adhesion and gastrulation. *Development*. 130:5339–5350. doi:10.1242/dev.00735[REMOVED HYPERLINK FIELD]

Severson, A.F., D.R. Hamill, J.C. Carter, J. Schumacher, and B. Bowerman. 2000. The aurora-related kinase AIR-2 recruits ZEN-4/CeMKLP1 to the mitotic spindle at metaphase and is required for cytokinesis. *Curr. Biol.* 10:1162–1171. doi:10.1016/S0960-9822(00)00715-6